Available online at www.sciencedirect.com
SCIENCE DIRECT®
Journal of Sound and Vibration 282 (2005) 1183–1199
JOURNAL OF SOUND AND VIBRATION
www.elsevier.com/locate/jsvi

Reconstruction of vibro-acoustic fields using hybrid nearfield acoustic holography

X. Zhao, S.F. Wu*

Department of Mechanical Engineering, Wayne State University, Detroit, MI 48202, USA

Received 28 March 2003; accepted 4 April 2004

Abstract

Hybrid nearfield acoustical holography is utilized to reconstruct the vibro-acoustic fields generated by an arbitrary structure vibrating in an unbounded fluid medium. This hybrid NAH is based on the modified Helmholtz equation least-squares method that expresses the field acoustic pressure in terms of expansions of outgoing and incoming waves. The expansion coefficients are determined by solving an over-determined linear system of equations obtained by matching the assumed-form solution to a finite number of acoustic pressures measured in the field via least squares. The measurements are taken over a conformal surface around the source at close range so that the evanescent waves can be captured. Once the expansion coefficients are specified, enough field acoustic pressures are regenerated on a conformal surface around the source and are taken as input to the Helmholtz integral formulation implemented numerically by the boundary element method. The acoustic pressure and normal velocity on the source surface are reconstructed using singular value decomposition, modified Tikhonov regularization and generalized cross-validation method. This hybrid NAH enables one to obtain a satisfactory reconstruction cost effectively because the majority of the input data are calculated but not measured. Numerical examples of reconstructing the vibro-acoustic quantities on the surfaces of an engine block and a highly elongated cylinder are demonstrated.

*Corresponding author. Tel.: +1-313-577-3884; fax: +1-313-577-8789.
E-mail address: sean_wu@wayne.edu (S.F. Wu).

0022-460X/$ - see front matter © 2004 Elsevier Ltd. All rights reserved.
doi:10.1016/j.jsv.2004.04.022

1. Introduction

Nearfield acoustical holography (NAH) [1–4] has shown a great promise in reconstructing the vibro-acoustic field generated by a vibrating structure based on acoustic pressures measured on a hologram plane. Traditional NAH is carried out via Fourier acoustics [5], which is suitable for separable geometry such as an infinite plane, an infinite cylinder, and a sphere in a free field. For an arbitrary source surface, the Helmholtz integral theory implemented by the boundary element method (BEM) seems to be a natural choice, which correlates the field acoustic pressure to vibro-acoustic quantities on a source surface. This inverse BEM (IBEM) has been used to reconstruct acoustic radiation by many researchers [6–11] because of its applicability to arbitrary surfaces.

One major drawback of IBEM is that it requires at least six nodes per wavelength to accurately describe the vibro-acoustic quantities on a source surface. Accordingly, one must take a comparable, although not necessarily equal, amount of measurements to determine the acoustic quantities on the discrete nodes. For a complex structure such as an engine vibrating at low-to-mid frequencies, the number of nodes needed can be huge. As a result, the measurements can be excessive and reconstruction can be very time consuming. Another shortcoming of IBEM is that it may fail to yield a unique solution when the frequency is close to the eigenfrequencies of the corresponding interior boundary value problem. Although this nonuniqueness difficulty can be overcome by combining exterior and interior integral formulations [12], numerical computations can become very complicated. Moreover, the presence of $1/R^2$ in the integrands tends to make numerical solutions unstable when measurements are taken at a very close range ($R \approx 0$), which is undesirable in NAH. Although there is a nonsingular integral formulation [13], the complexities make it much less appealing than the original Helmholtz integral formulation.

In 1997, another NAH method was developed in which the acoustic pressure is expressed in terms of an expansion of the particular solutions to the Helmholtz equation. The coefficients of expansion are determined by matching an assumed-form solution to measured acoustic pressures through least squares; thus it is known as the Helmholtz equation least squares (HELS) method [14,15]. Since HELS solves the Helmholtz equation directly, it is immune to the nonuniqueness difficulty inherent in IBEM.

The main advantages of HELS are its simplicity in mathematical formulation, efficiency in numerical computation, and flexibility in engineering application. HELS has been successfully employed to reconstruct acoustic radiation from arbitrary structures in the exterior [16,17] and interior [18,19] regions. Moreover, it enables one to reconstruct the radiated acoustic fields with relatively few measurements or conduct a piece-wise reconstruction. However, HELS is not ideal for a highly irregular surface because of slow convergence of the expansion solution [20].

To improve the accuracy and efficiency of reconstruction, hybrid NAH is developed [21]. This hybrid NAH is based on a modified HELS formulation that expresses the acoustic pressure in terms of expansions of both outgoing and incoming waves. This modified HELS is combined with IBEM. The difference between hybrid NAH and CHELS method [22] is that the former allows regeneration of acoustic pressures on a conformal surface at very close range to a source surface so that the accuracy and efficiency of reconstruction are guaranteed, whereas the latter allows

regeneration of acoustic pressures on a hypothetical sphere enclosing the source structure. Consequently, the near-field information may be lost in CHELS, which is especially true for an elongated object, and the resulting reconstruction accuracy may be low.

In this paper, we apply hybrid NAH to reconstruction of the vibro-acoustic quantities on an arbitrarily shaped structure and a highly elongated cylinder. In particular, we show that hybrid NAH can yield satisfactory reconstruction with relatively few measurements. When these same measurements are used in IBEM alone, aliasing can occur and the reconstructed vibro-acoustic images can be greatly distorted.

2. Hybrid NAH

The basis of hybrid NAH is a modified HELS formulation, which expresses the acoustic pressure radiated from an arbitrary object vibrating at a constant frequency ω in an unbounded fluid medium as [21]

$$\{p(\mathbf{x};\omega)\} = [\Psi^{(1)}]\{C\} + [\Psi^{(2)}]\{D\}, \tag{1}$$

where $\Psi_{ij}^{(1)}$ and $\Psi_{ij}^{(2)}$ are the particular solutions to the Helmholtz equation. Using the spherical coordinates, we can write $\Psi_{ij}^{(1)}$ and $\Psi_{ij}^{(2)}$ as

$$\Psi_{ij}^{(1)} \equiv \Psi_{nl}^{(1)}(r,\theta,\phi;\omega) = h_n^{(1)}(kr)\,Y_n^{(l)}(\theta,\phi) \text{ and } \Psi_{ij}^{(2)} \equiv \Psi_{nl}^{(2)}(r,\theta,\phi;\omega) = h_n^{(2)}(kr)\,Y_n^{l}(\theta,\phi), \tag{2}$$

where $h_n^{(1)}(kr)$ and $h_n^{(2)}(kr)$ represent the spherical Hankel functions of order n of the first and second kinds, respectively, $k = \omega/c$ is the acoustic wavenumber with c being the speed of sound of the fluid medium and $Y_n^l(\theta,\phi)$ are the spherical harmonics. The indices j, n, and l in Eq. (2) are related together through $j = n^2 + n + l + 1$, with n starting from 0 to N_0 and l varying from $-n$ to $+n$. Thus, for each n and l we have $j = 1$ to J, where J is the number of expansion terms $J = (N_0 + 1)^2$.

Physically, the terms on the right side of Eq. (1) represent the outgoing and incoming spherical waves, respectively. The completeness of an expansion of the particular solutions to the Helmholtz equation is provided by Vekua [23]. Eq. (1) makes sense when we attempt to project the acoustic field back toward an arbitrarily shaped source based on acoustic pressures measured on a conformal surface at very close range to a source surface. When reconstruction of acoustic radiation from a spherical surface in a free field is desired, we should set $D_j = 0$ in Eq. (1) for there is no incoming wave.

For convenience, we combine the expansion functions in Eq. (1) into a single matrix and determine the corresponding coefficients by solving an over-determined linear system of equations obtained by matching the assumed-form solution to the measured acoustic pressures through least squares:

$$[A]_{M\times 2J}\{\hat{C}\}_{2J\times 1} = \{p(\mathbf{x};\omega)\}_{M\times 1}, \tag{3}$$

where M is the number of field acoustic pressures ($M \geqslant 2J$); the matrix $[A]$ and coefficients $\{\hat{C}\}$ are defined by

$$[A]_{M\times 2J} = \begin{bmatrix} \Psi_{11}^{(1)} & \Psi_{11}^{(2)} & \Psi_{12}^{(1)} & \Psi_{12}^{(2)} & \cdots & \Psi_{1J}^{(1)} & \Psi_{1J}^{(2)} \\ \Psi_{21}^{(1)} & \Psi_{21}^{(2)} & \Psi_{22}^{(1)} & \Psi_{22}^{(2)} & \cdots & \Psi_{2J}^{(1)} & \Psi_{2J}^{(2)} \\ \vdots & \vdots & \vdots & \vdots & \ddots & \vdots & \vdots \\ \Psi_{J1}^{(1)} & \Psi_{J1}^{(2)} & \Psi_{J2}^{(1)} & \Psi_{J2}^{(2)} & \cdots & \Psi_{JJ}^{(1)} & \Psi_{JJ}^{(2)} \\ \vdots & \vdots & \vdots & \vdots & \ddots & \vdots & \vdots \\ \Psi_{M1}^{(1)} & \Psi_{M1}^{(2)} & \Psi_{M2}^{(1)} & \Psi_{M2}^{(2)} & \cdots & \Psi_{MJ}^{(1)} & \Psi_{MJ}^{(2)} \end{bmatrix}_{M\times 2J} \quad \text{and} \quad \{\hat{C}\}_{2J\times 1} = \begin{Bmatrix} C_1 \\ D_1 \\ C_2 \\ D_2 \\ \vdots \\ C_J \\ D_J \end{Bmatrix}_{2J\times 1}. \tag{4}$$

It is worth pointing out that one can take fewer measurements (equations) than expansion functions (unknowns), namely, $M < 2J$, and use singular value decomposition (SVD) to solve Eq. (3). However, the solutions thus obtained may be mathematically nonunique because the missing equations are replaced by null space. Moreover, aliasing may occur when measurements are too few [20]. Therefore, we always take sufficient number of measurements in NAH.

In practice, the matrix $[A]$ in Eq. (3) may be ill conditioned either due to measurement errors or due to an insufficient number of measurements being taken. Therefore, we need to truncate the expansion (3) at an optimal number of terms J_{op}. To this end, we take M_1 measurements of acoustic pressures $p(\mathbf{x}_m;\omega)$ on a conformal surface Γ around the source at close range, and use part of the measured data M_0 ($M_0 < M_1$) to solve the expansion coefficients $\{\hat{C}\}$. Next, we minimize residues with respect to M_1 measurements taken on Γ using Eq. (3). Mathematically, we can write this process as

$$\min_{\hat{C}_1,\hat{C}_2,\ldots,\hat{C}_J} ||p_J(\mathbf{x}_m^{\Gamma};\omega) - p(\mathbf{x}_m^{\Gamma};\omega)||_2, \quad \mathbf{x}_m^{\Gamma} = \{x_1^{\Gamma}, x_2^{\Gamma}, \ldots, x_{M_0}^{\Gamma}\}^{\mathrm{T}}, \quad x_i^{\Gamma} \in \Gamma, \quad i = 1 \text{ to } M_0, \tag{5a}$$

$$\min_{J} ||p_J(\mathbf{x}_m^{\Gamma};\omega) - p(\mathbf{x}_m^{\Gamma};\omega)||_2, \quad \mathbf{x}_m^{\Gamma} = \{x_1^{\Gamma}, x_2^{\Gamma}, \ldots, x_{M_1}^{\Gamma}\}^{\mathrm{T}}, \quad x_i^{\Gamma} \in \Gamma, \quad i = 1 \text{ to } M_1. \tag{5b}$$

Note that the value of J_{op} thus obtained is optimized with respect to a particular set of measurements and changes with the excitation frequency. Also, since the acoustic pressures are regenerated on the surface Γ but not projected back toward the source surface, no regularization is needed. The optimal expansion coefficients $\hat{C}_j$, $j = 1$ to J_{op}, can provide a best approximation of the field acoustic pressures on the surface Γ. The accuracy of regenerated acoustic pressures is consistent with that of the actual measured data, provided that sufficient measurements M_1 are taken. This is because we can expand any radiating solution in terms of the particular solutions to the Helmholtz equation [24] and such an expansion is complete and convergent [23].

Suppose that we want to reconstruct the vibro-acoustic quantities on an arbitrarily shaped source surface. A natural approach is to use the Helmholtz integral theory that correlates the field acoustic pressure to surface acoustic quantities. This Helmholtz integral formulation can be solved numerically using BEM by discretizing the surface into elements with N nodes, and the surface acoustic quantities on these discrete nodes can be determined by taking N (or more)

measurements.

$$[T_p]_{N\times N}\{p(\mathbf{x}_S;\omega)\}_{N\times 1} = \{p(\mathbf{x}_m;\omega)\}_{N\times 1}, \tag{6a}$$

$$[T_v]_{N\times N}\{v_n(\mathbf{x}_S;\omega)\}_{N\times 1} = \{p(\mathbf{x}_m;\omega)\}_{N\times 1}, \tag{6b}$$

where $[T_p]$ and $[T_v]$ represent the transfer matrices that correlate the field acoustic pressures to surface acoustic pressures and surface normal velocities, respectively, which are given by [10]

$$[T_p]_{N\times N} = [M]_{N\times N}[M_S]^{-1}_{N\times N}[D_S]_{N\times N} + [D]_{N\times N}, \tag{7a}$$

$$[T_v]_{N\times N} = [D]_{N\times N}[D_S]^{-1}_{N\times N}[M_S]_{N\times N} + [M]_{N\times N}, \tag{7b}$$

and where $[M]$ and $[D]$ imply the effects of monopoles and dipoles at a field point, respectively, $[M_S]$ and $[D_S]$ represent those of monopoles and dipoles at a surface point, respectively.

In general, the number of discrete nodes N necessary to describe the vibro-acoustic field on an arbitrarily shaped source surface is very large. If a comparable amount of measurements is taken, the reconstruction process can be very time consuming and complex. The main advantage of hybrid NAH lies in the fact that we only need to take a finite number of measurements, say, M_1 ($M_1 \ll N$), and then use Eq. (5) to determine the optimal expansion coefficients $\hat{C}_j$, $j = 1$ to J_{op}. Once this is done, we can use Eq. (3) to regenerate N field acoustic pressures and take them as input to Eq. (6) to determine the surface acoustic quantities on N discrete nodes.

Note that Eq. (6) is a discretized Fredholm integral equation of the first kind, which is mathematically ill posed when source terms under the integral sign are sought based on the input data specified on the left side [25–28]. To overcome this difficulty, we use SVD to expand the transfer matrices $[T_p]$ and $[T_v]$ in terms of the dominant acoustic modes:

$$\{p(\mathbf{x}_S;\omega)\}_{N\times 1} = [V_p]_{N\times N}[\Sigma_p]^{-1}_{N\times N}[U_p]^H_{N\times N}\{p(\mathbf{x}_m;\omega)\}_{N\times 1}, \tag{8a}$$

$$\{v_n(\mathbf{x}_S;\omega)\}_{N\times 1} = [V_v]_{N\times N}[\Sigma_v]^{-1}_{N\times N}[U_v]^H_{N\times N}\{p(\mathbf{x}_m;\omega)\}_{N\times 1}, \tag{8b}$$

where $[U_p]$ and $[V_p]$ are unitary matrices that contain the left and right singular vectors of $[T_p]$, respectively, $[U_v]$ and $[V_v]$ are unitary matrices that contain the left and right singular vectors of $[T_v]$, respectively, $[\Sigma_p]$ and $[\Sigma_v]$ are the diagonal matrices that contain the singular values of $[T_p]$ and $[T_v]$, respectively, and $p(\mathbf{x}_m;\omega)$ on the right side of Eq. (8) are regenerated by

$$\{p(\mathbf{x}_m;\omega)\}_{N\times 1} = [A]_{N\times 2J_{\text{op}}}[A]^{\dagger}_{M_0\times 2J_{\text{op}}}\{p(\mathbf{x}_{m'};\omega)\}_{M_0\times 1}, \tag{9}$$

where $[A]^{\dagger}$ is a pseudo-inversion of $[A]$, and the symbols $\mathbf{x}_{m'}$ and $\mathbf{x}_m$ represent the actual measurement points and points to be regenerated, respectively.

Eqs. (8) and (9) show that the surface acoustic pressure $p(\mathbf{x}_S;\omega)$ and the surface normal velocity $v_n(\mathbf{x}_S;\omega)$ on N nodes of an arbitrarily shaped surface can now be reconstructed by M_1 measurements (M_0 measurements are used to specify the expansion coefficients, and M_1 measurements to determine an optimal number of expansions J_{op}; see Eq. (5)). Since $M_1 \ll N$, the measurement complexities and time are significantly reduced and reconstruction efficiency is greatly enhanced.

3. Regularization

In most NAH applications the measured acoustic pressures are inaccurate and incomplete and the resulting transfer matrices in Eq. (7) are ill conditioned. A common regularization is via Tikhonov regularization (TR) [26,28]:

$$J(\mathbf{v}^{\delta,\alpha}) = ||\mathbf{T}\mathbf{v}^{\delta} - \mathbf{p}^{\delta}||_2^2 + \alpha||\mathbf{L}\mathbf{v}^{\delta}||_2^2, \tag{10}$$

where $\mathbf{v}^{\delta,\alpha}$ represents the reconstructed field which depends on the regularization parameter α, $\mathbf{p}^{\delta}$ implies a set of input data, $\mathbf{v}^{\delta}$ is the source field to be reconstructed, $\mathbf{T}$ is a transfer function that correlates $\mathbf{v}^{\delta}$ to $\mathbf{p}^{\delta}$, and $\mathbf{L}$ is an identity matrix for standard TR and equal to a filtered matrix for a modified TR. The first term on the right side of Eq. (10) represents an ultra rough least-squares solution where $\alpha = 0$, while the second term implies an ultra smooth solution where $\alpha \to \infty$. Thus, the choice of α in Eq. (10) allows one to decide how far to go to achieve a certain smoothness.

Once the regularization format is selected, the next step is to determine the value of α. In this paper, we select the generalized cross-validation (GCV) method [29] to determine α. The basic idea of GCV is to leave a particular measured acoustic pressure out of calculations of the cost function first, and then evaluate the effectiveness of the reconstructed source field in predicting the value of the omitted data. This process is repeated for all the data points.

Note that in this paper, we assume that noise contained in the measured acoustic pressure is random with zero variance. This characteristic is retained in the regenerated acoustic pressures and therefore the assumption of white noise in GCV is not violated.

Using TR and GCV, we can rewrite Eq. (8) and reconstructed surface acoustic pressure $\mathbf{p}^{\delta,\alpha}$ and surface normal velocity $\mathbf{v}_n^{\delta,\alpha}$ as [28,30]

$$\mathbf{p}^{\delta,\alpha} = V_p F_p^{\alpha} \Sigma_p^{-1} U_p^H \mathbf{p}^{\delta} \quad \text{and} \quad \mathbf{v}_n^{\delta,\alpha} = V_v F_v^{\alpha} \Sigma_v^{-1} U_v^H \mathbf{p}^{\delta}, \tag{11}$$

where F_p^{α} and F_v^{α} are the diagonal matrices that act as the low-pass filters devised to eliminate the high wavenumbers in reconstructing $\mathbf{p}^{\delta,\alpha}$ and $\mathbf{v}_n^{\delta,\alpha}$, respectively.

$$F_p^{\alpha} = \operatorname{diag}\left(\cdots, \quad \frac{\sigma_{p,j}^2}{\alpha + \sigma_{p,j}^2}, \cdots\right) \quad \text{and} \quad F_v^{\alpha} = \operatorname{diag}\left(\cdots, \quad \frac{\sigma_{v,j}^2}{\alpha + \sigma_{v,j}^2}, \quad \cdots\right), \tag{12}$$

where subscripts p and v imply acoustic pressure and normal surface velocity, respectively, $\sigma_{p,j}$ and $\sigma_{v,j}$ are the jth singular values of $\mathbf{T}_p$ and $\mathbf{T}_v$ defined, respectively, in Eq. (7).

Note that the standard TR tends to limit the growth of all wavenumber components. Since distortion in reconstruction is primarily caused by the high wavenumber components (evanescent waves), it is logical to suppress the evanescent waves while leaving low wavenumber components unchanged. Hence, we modify the penalty function in Eq. (10) by restricting the growth of the evanescent waves and rewrite the reconstructed acoustic quantities as

$$\mathbf{p}^{\delta,\alpha} = V_p F_{p,M}^{\alpha} \Sigma_p^{-1} U_p^H \mathbf{p}^{\delta} \quad \text{and} \quad \mathbf{v}_n^{\delta,\alpha} = V_v F_{v,M}^{\alpha} \Sigma_v^{-1} U_v^H \mathbf{p}^{\delta}, \tag{13}$$

where $F_{p,M}^{\alpha}$ and $F_{v,M}^{\alpha}$ are the low-pass filters in the modified TR that are given, respectively, by

$$F_{p,M}^{\alpha} = \operatorname{diag}\left(\frac{\sigma_{p,j}^2}{\alpha^3/(\alpha + \sigma_{p,j}^2)^2 + \sigma_{p,j}^2}\right) \quad \text{and} \quad F_{v,M}^{\alpha} = \operatorname{diag}\left(\frac{\sigma_{v,j}^2}{\alpha^3/(\alpha + \sigma_{v,j}^2)^2 + \sigma_{v,j}^2}\right). \tag{14}$$

The regularization parameter α is determined by GCV through a minimization process

$$\min\left(\frac{||F_{h,M}^{\alpha}U_p^H\mathbf{p}^{\delta}||_2^2}{[\mathrm{Tr}(F_{h,M}^{\alpha})]^2}\right), \tag{15}$$

where $F_{h,M}^{\alpha}$ implies a high-pass filter for the modified TR defined as

$$F_{h,M}^{\alpha} \equiv \mathbf{I} - F_{p,M}^{\alpha} = \mathrm{diag}\left(\cdots, \frac{\alpha}{\alpha + \sigma_{p,j}^2(\alpha+\sigma_{p,j}^2)^2/\alpha^2}, \cdots\right), \tag{16a}$$

for reconstructing acoustic pressure, or

$$F_{h,M}^{\alpha} \equiv \mathbf{I} - F_{v,M}^{\alpha} = \mathrm{diag}\left(\cdots, \frac{\alpha}{\alpha + \sigma_{v,j}^2(\alpha+\sigma_{v,j}^2)^2/\alpha^2}, \cdots\right), \tag{16b}$$

for reconstructing normal surface velocity. The symbol $\mathbf{I}$ represents an identity matrix.

Note that one can use other regularization techniques such as standard TR or Landweber iterations [31] together with Morozov's discrepancy principle (MDP) [32] to reconstruct vibro-acoustic quantities. Numerical tests demonstrate, however, that GCV may fail to yield a value of α when coupled with standard TR. While MDP can yield a value of α, its accuracy may not be very good when coupled with standard TR. In a separate paper, we considered several different regularization and parameter choice methods, including the L-curve method, and their combinations with various penalty functions in order to determine an optimal regularization scheme for a general inverse acoustic radiation problem [33]. In this study, we only tested a limited number of combinations of regularization and parameter choice methods and an optimal combination seems to be a modified TR and GCV.

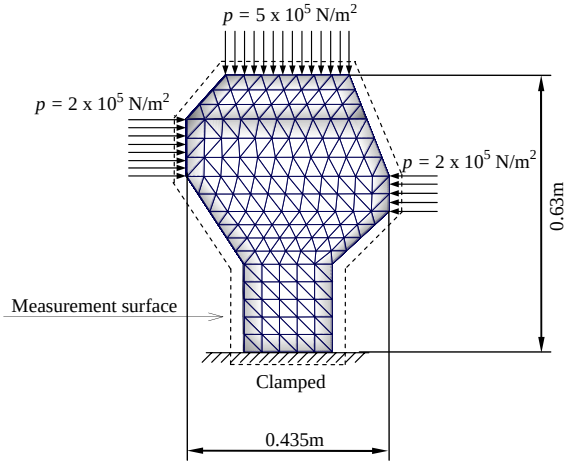

Fig. 1. Schematic of a simplified engine block subject to harmonic pressure force excitations.

4. Numerical examples

We now use hybrid NAH to reconstruct the vibro-acoustic quantities on the surfaces of arbitrary objects vibrating in an unbounded fluid medium. In particular, we want to show the enhancement of reconstruction efficiency and accuracy as compared with those of IBEM alone.

The first example is a simplified four-cylinder engine block. Here the block is assumed to be clamped at the bottom and subject to harmonic excitations of uniformly distributed pressures on three arbitrarily selected surfaces: $5 \times 10^5\,\mathrm{N/m^2}$ on top and $2 \times 10^5\,\mathrm{N/m^2}$ on the protruding parts of the front and back surfaces (see Fig. 1). The overall dimensions of the engine are 0.435 m in the x-axis direction, 0.46 m in the y-axis direction, and 0.63 m in the z-axis direction.

In carrying out numerical computations, the engine block is divided into 1530 six-node wedge solid elements and first-order brick solid elements with a total of 1878 nodes. The normal surface

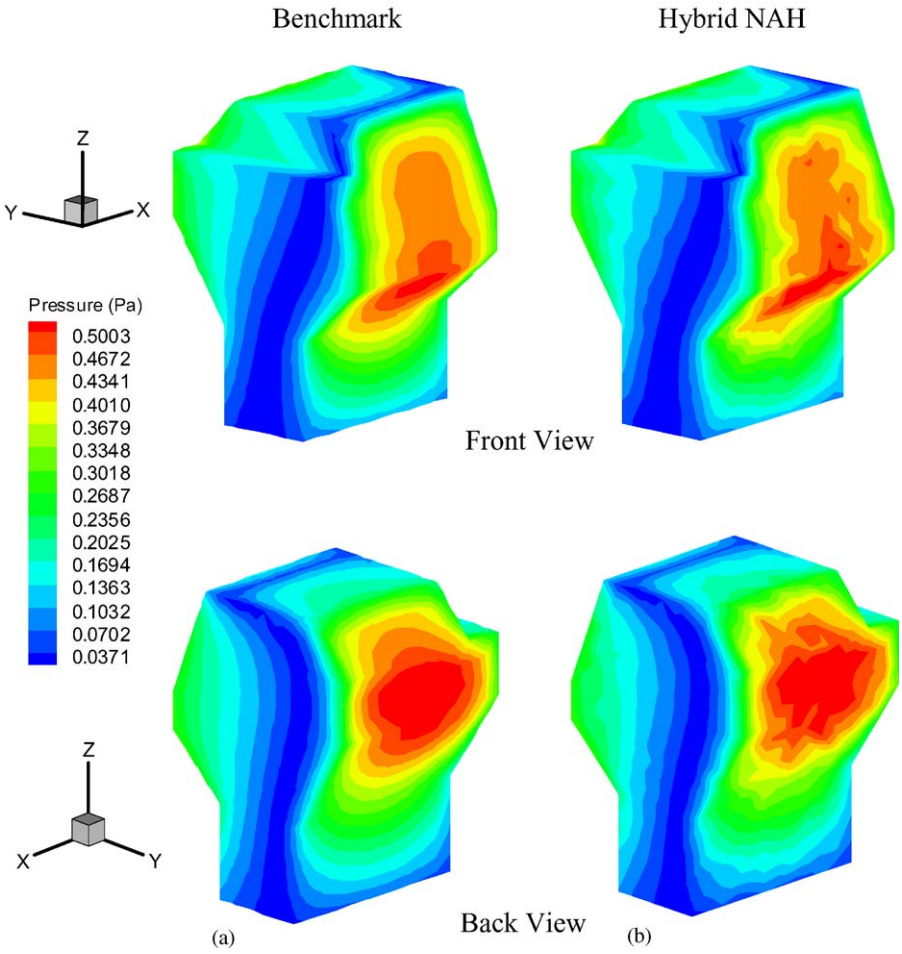

Fig. 2. Comparison of surface acoustic pressure distributions on the engine block at $ka = 1$. (a) Benchmark values; (b) reconstructed using hybrid NAH with 388 input data.

velocities on these nodes are calculated using commercial software NASTRAN®. Once this is done, the surface acoustic pressures are calculated using BEM with 1548 linear triangular elements with 776 nodes. Having determined the normal surface velocity and surface acoustic pressure, we specify the field acoustic pressures on certain discrete points on a conformal surface around the engine block. If IBEM alone is used to reconstruct the vibro-acoustic quantities on the entire surface, we would need to take nearly 776 measurements to determine these unknowns on all 776 discrete nodes.

To show the effectiveness of hybrid NAH, we half the acoustic pressure measurements to 388. These reduced input data are used in Eq. (5) to determine optimal expansion coefficients. Once this is done, Eq. (3) is employed to regenerate 776 field acoustic pressures on a conformal surface around the engine at a 5 mm clearance, and then substitute them in Eq. (13) to reconstruct the surface acoustic quantities. These reconstructed quantities are compared with the surface acoustic pressures produced by BEM and the normal surface velocities provided by FEM results. Numerical tests are conducted at various dimensionless frequencies. For brevity, only the results

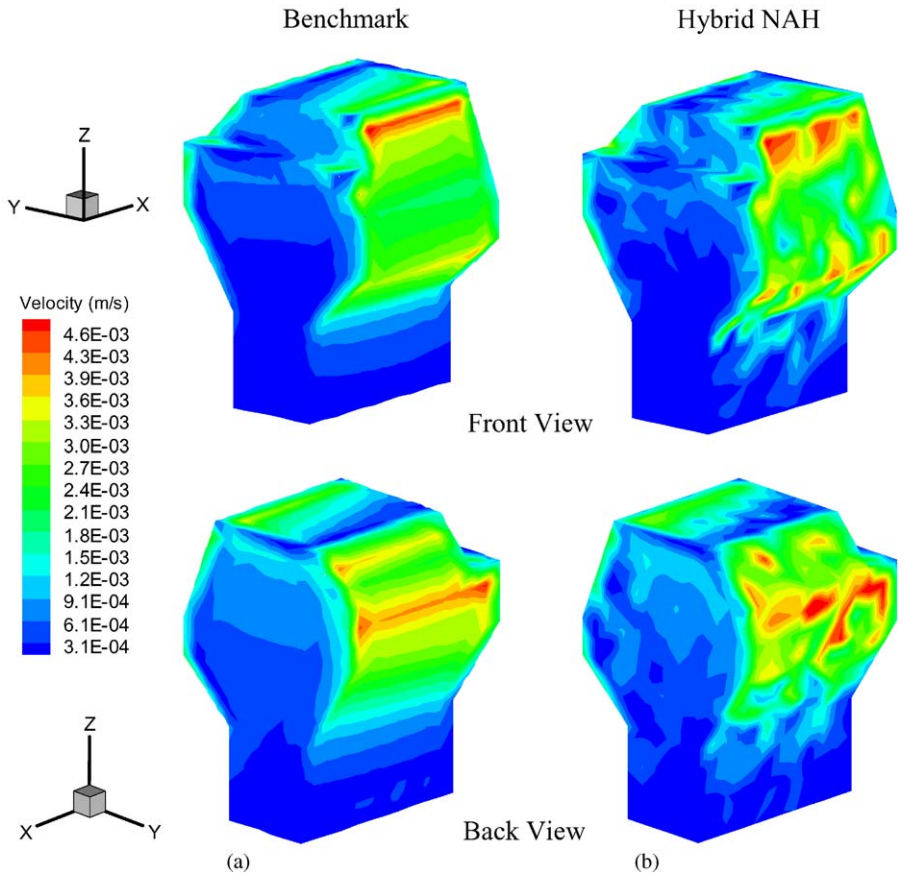

Fig. 3. Comparison of normal surface velocity distributions on the engine block at $ka = 1$. (a) Benchmark values; (b) reconstructed using hybrid NAH with 388 input data.

at $ka = 1$ and 2 are shown below. The optimal number of expansion functions at $ka = 1$ is found to be $J_{op} = 25$ and that at $ka = 2$ is $J_{op} = 31$.

Figs. 2 and 3 depict comparisons of the reconstructed surface acoustic pressure and the surface normal velocity against the benchmark data, respectively, at $ka = 1$. Similar comparisons of the reconstructed vibro-acoustic quantities and benchmark data on the engine block surface at $ka = 2$ are displayed in Figs. 4 and 5. Satisfactory reconstruction is obtained in all cases. For completeness, we also illustrate the comparisons of the surface acoustic pressures reconstructed by using IBEM alone under the same 388 input data as those used in hybrid NAH at $ka = 1$. Since the number of discrete nodes is twice as many as the input data, the system of Eq. (6) is greatly under determined and a satisfactory reconstruction may not be guaranteed.

If a matrix is severely ill conditioned, the singular values decay very fast. Under this condition, it will still be possible to use SVD to expand the matrix in terms of the dominant acoustic modes and obtain a satisfactory reconstruction. However, if a matrix is not very ill conditioned (as in the case of reconstructing the surface acoustic pressure), the singular values decay slowly. If the input

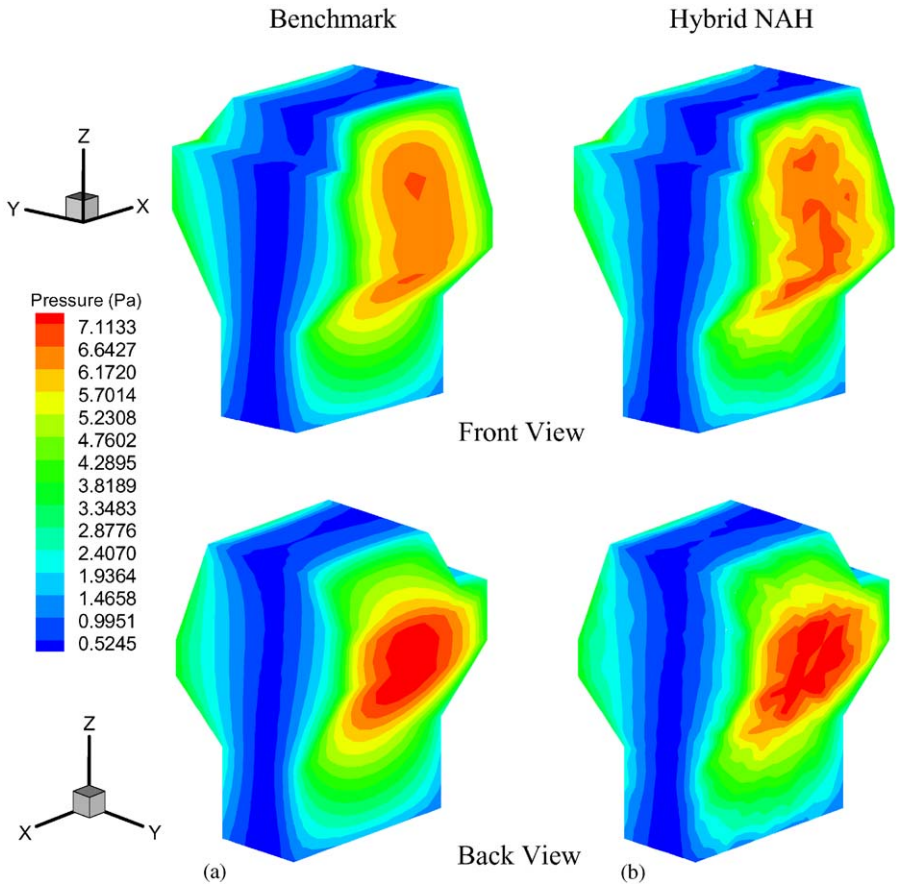

Fig. 4. Comparison of surface acoustic pressure distributions on the engine block at $ka = 2$. (a) Benchmark values; (b) reconstructed using hybrid NAH with 388 input data.

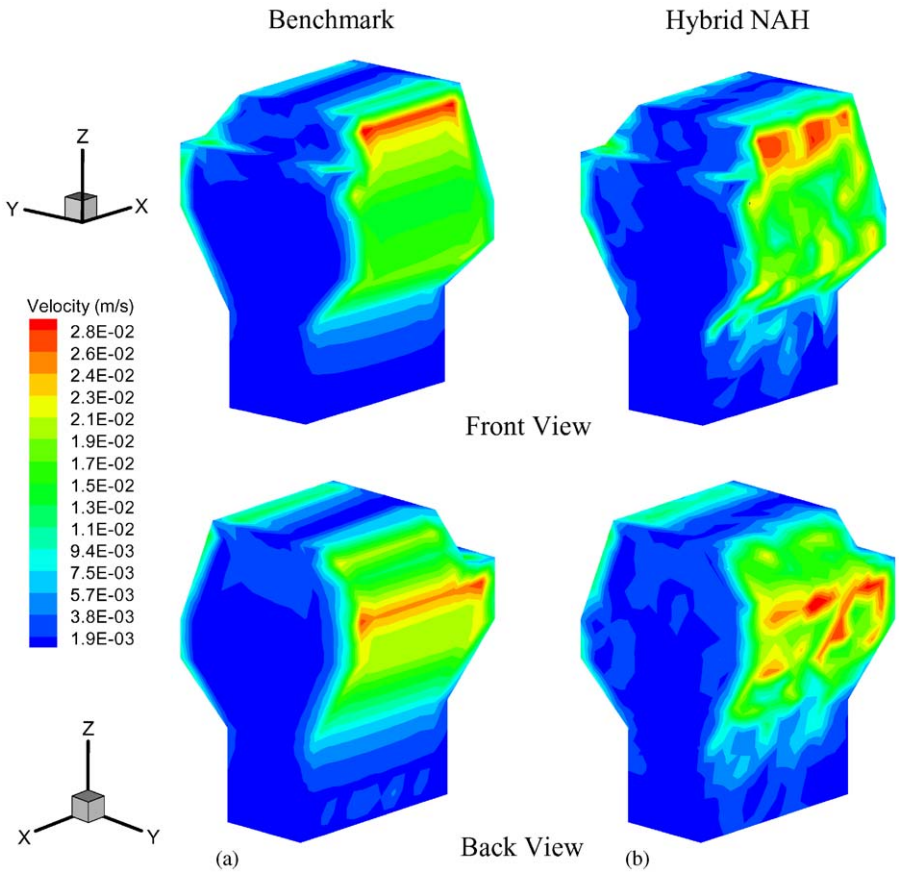

Fig. 5. Comparison of normal surface velocity distributions on the engine block at $ka = 2$. (a) Benchmark values; (b) reconstructed using hybrid NAH with 388 input data.

data are not sufficient and truncation has to be made, some vital information will necessarily be lost. Under this condition, there is no way of getting a good reconstruction and aliasing in the reconstructed image will occur [21] (see Fig. 6).

The second example is an elongated circular cylinder with two spherical end caps (see Fig. 7(a)). To examine the effectiveness of hybrid NAH, we select a large aspect ratio $b/a = 10$, where a and b are the radius and half-length of the cylinder, respectively.

Since there are no closed-form solutions for this elongated cylinder, BEM codes are used to generate the benchmark data on the source surface and in the field on a conformal surface with a 5 mm clearance. In carrying out numerical computations, the cylinder is discretized into 1008 triangular elements with 506 nodes (see Fig. 7(b)). The normal velocity on cylindrical surface is selected and the surface acoustic pressures are calculated using BEM codes. Once this is done, the field acoustic pressures on a conformal surface are obtained using Eq. (6b) and are taken as input to hybrid NAH formulas to reconstruct vibro-acoustic quantities on the cylindrical surface.

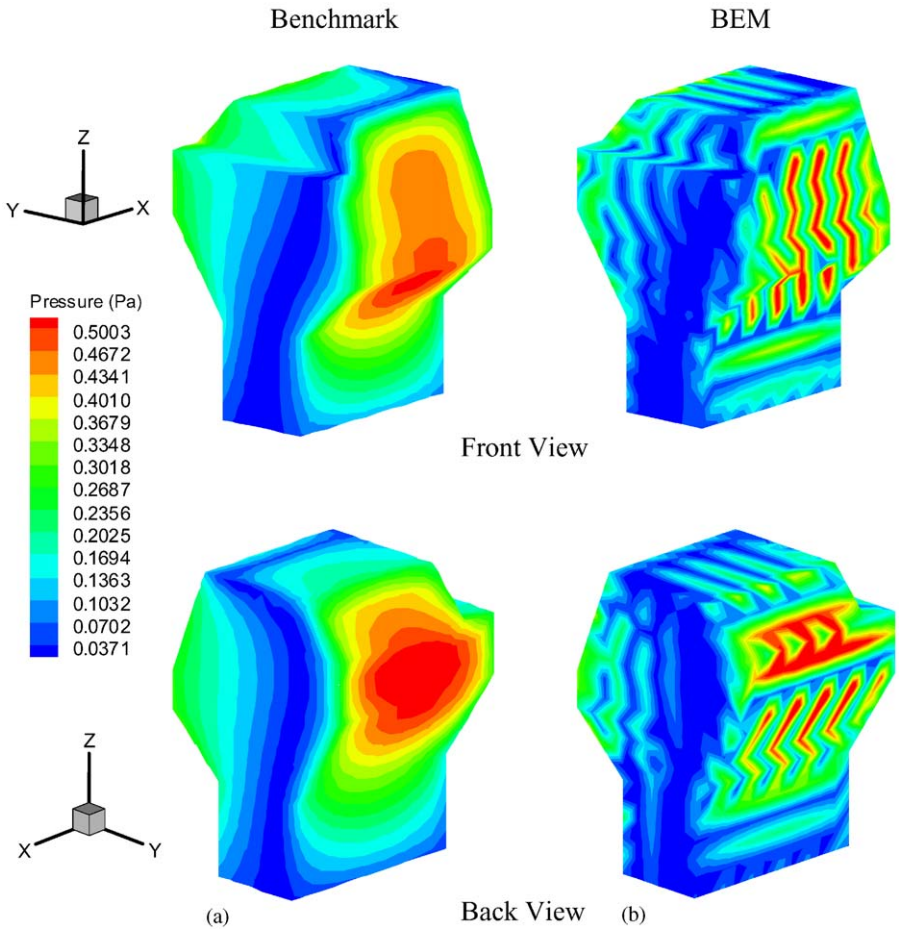

Fig. 6. Comparison of surface acoustic pressure distributions on the engine block at $ka = 1$. (a) Benchmark values; (b) reconstructed using BEM-based NAH with 388 input data.

In what follows, we first consider a dilating cylinder of radius $a = 0.1$ m with a uniform surface normal velocity $V_0 = 0.01$ m/s at $ka = 1$. Note that in this case we conduct a piece-wise reconstruction, namely, calculating the optimal expansion coefficients C_j for two spherical ends first, and then C_j and D_j for the cylindrical surface.

Specifically, we take $M_1 = 10$ field measurements that are evenly distributed over a half spherical surface concentric to the left spherical endcap. Half of these data ($M_0 = 5$) are used as input to Eq. (5) to solve the expansion coefficients C_j and the rest is used to optimize the number of expansion terms, which is $J_{\text{op}} = 5$. These procedures are followed in determining the optimal expansion coefficients for the right spherical endcap. In carrying out numerical computations, the origins are set at O_1 and O_2 for the left and right endcaps (see Fig. 7(a)), respectively. Once this is done, we use Eq. (3) to regenerate additional 19 field acoustic pressures on these two half spherical conformal surfaces and take them as input to reconstruct the vibro-acoustic quantities on the spherical endcaps.

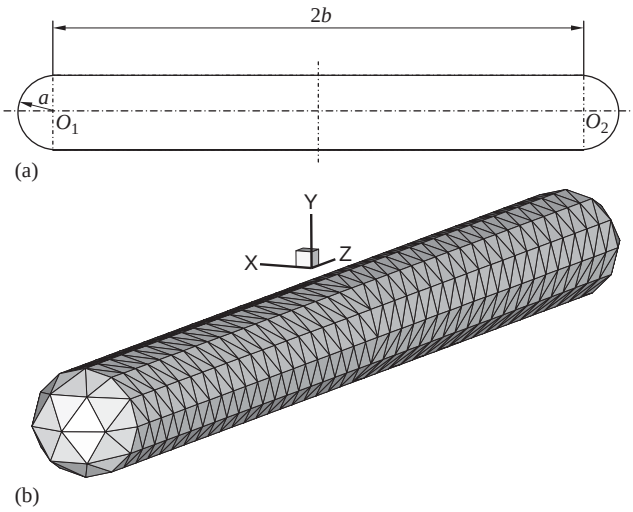

Fig. 7. A cylinder with two spherical endcaps. (a) Schematic; (b) discretization.

In a similar manner, we take $M_1 = 234$ field measurements that are evenly distributed on a concentric cylindrical surface and use Eq. (5) to get the optical expansion terms, $J_{\text{op}} = 46$, and the corresponding expansion coefficients C_j and D_j. Next, we utilize Eq. (3) to regenerate 468 additional field acoustic pressures and take all of them as input to Eq. (13) to reconstruct acoustic pressures and normal velocities on the cylindrical surface.

Since the acoustic field is axisymmetric, the results obtained are only presented along the generator of the cylinder. Figs. 8(a) and 8(b) show the comparisons of the reconstructed surface acoustic pressures and normal surface velocities versus the benchmark values, respectively, at $ka = 1$. Similar comparisons of the reconstructed vibro-acoustic quantities and benchmark data on the surface of the cylinder oscillating back and forth along the z-axis with velocity amplitude $V_a = 0.01\,\text{m/s}$ at $ka = 1$ are displayed in Figs. 8(c) and 8(d), respectively. Note that the optimal numbers of expansion functions in this case are found to be the same as those of the dilating cylinder at both spherical ends, namely, $J_{\text{op}} = 5$. The optimal number of expansion functions for the cylindrical surface is $J_{\text{op}} = 55$. Satisfactory reconstruction is obtained in both cases.

For comparison purpose, we also demonstrate reconstruction of vibro-acoustic quantities on the surface of the cylinder using IBEM alone (see Fig. 9) with $M_1 = 253$, which is equal to one half of the discrete nodes on the source surface ($N = 506$). The same regularization and parameter choice method as those in hybrid NAH are used. Since the matrix for reconstructing surface acoustic pressure is not very ill conditioned, the singular values decay slowly. Under this condition, a truncated SVD with insufficient input data will necessarily discard vital information and the resultant reconstructed image will be distorted. On the other hand, the matrix for normal surface velocity is severely ill conditioned and the corresponding singular values decay very fast. Under this condition, it is still possible to use a truncated SVD to get satisfactory reconstruction of the normal surface velocity.

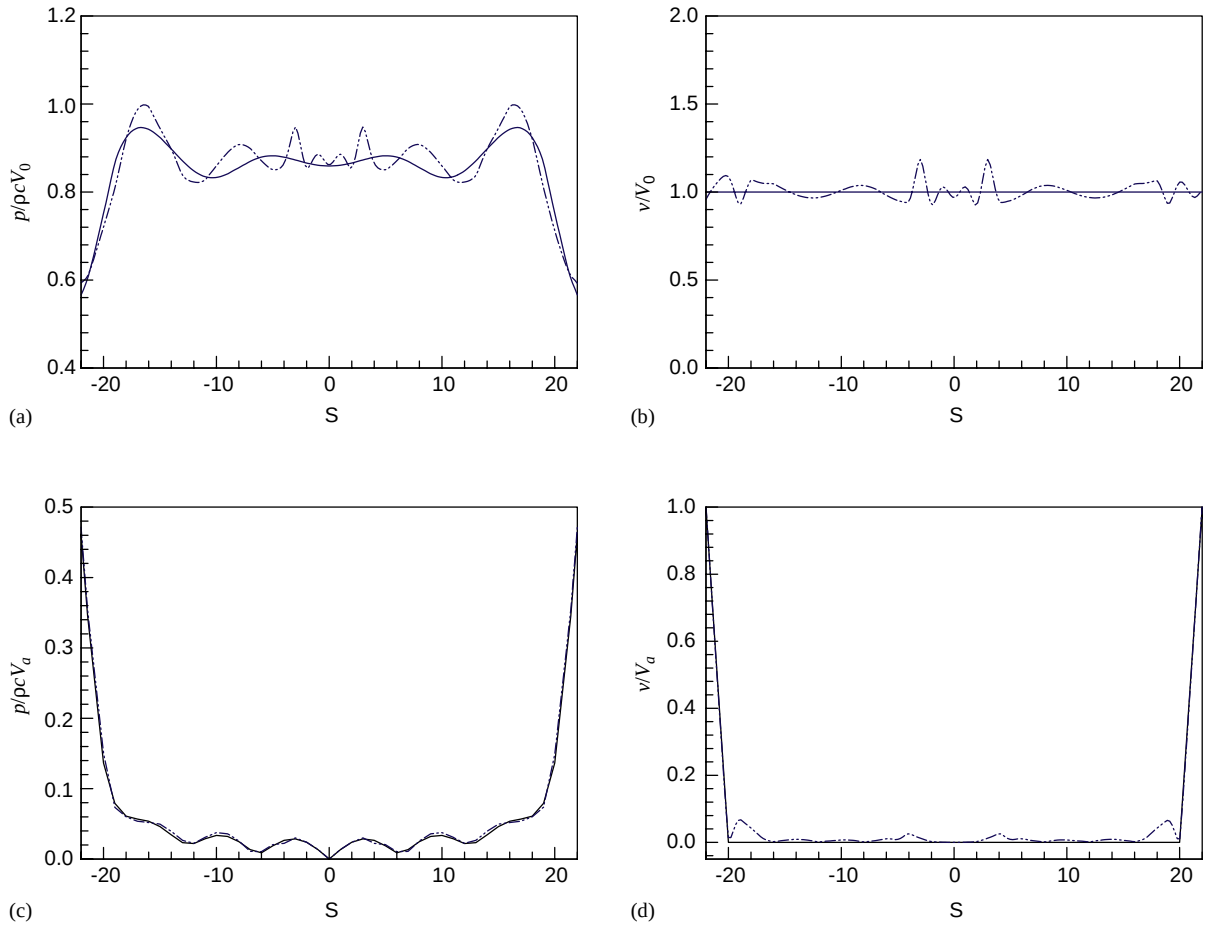

Fig. 8. Comparisons of dimensionless vibro-acoustic distributions on the surface of a cylinder with two spherical endcaps and a large half-length to radius aspect ratio $b/a = 10$ at $ka = 1$: — benchmark; $-\cdots-$ hybrid NAH. (a) Surface acoustic pressure for dilating $ka = 1$ case; (b) surface normal velocity for dilating case; (c) surface acoustic pressure $ka = 1$ for oscillating case; (d) surface normal velocity for oscillating case.

The hybrid NAH also allows one to determine the critical wavenumber that separate the propagating components of the acoustic waves from the nonpropagating ones. Fig. 10 shows the "k-space" interpretation of typical modes obtained from SVD and a two-dimensional discrete Fourier transform in the axial and circumferential directions. Here red and blue indicate positive and negative values, respectively, and ellipses represent the critical radius beyond which there is no acoustic radiation to the far field. These results indicate that to suppress sound one only needs to concentrate on the acoustic modes that fall inside the critical radius (see Fig. 10(a)) because they are responsible for acoustic radiation to the far field. The modes that fall outside the critical radius (see Fig. 10(b)) represent nonpropagating modes. The capability of NAH to identify the modes that are responsible for acoustic radiation is a remarkable advantage in diagnosing the vibro-acoustic sources of a complex vibrating structure.

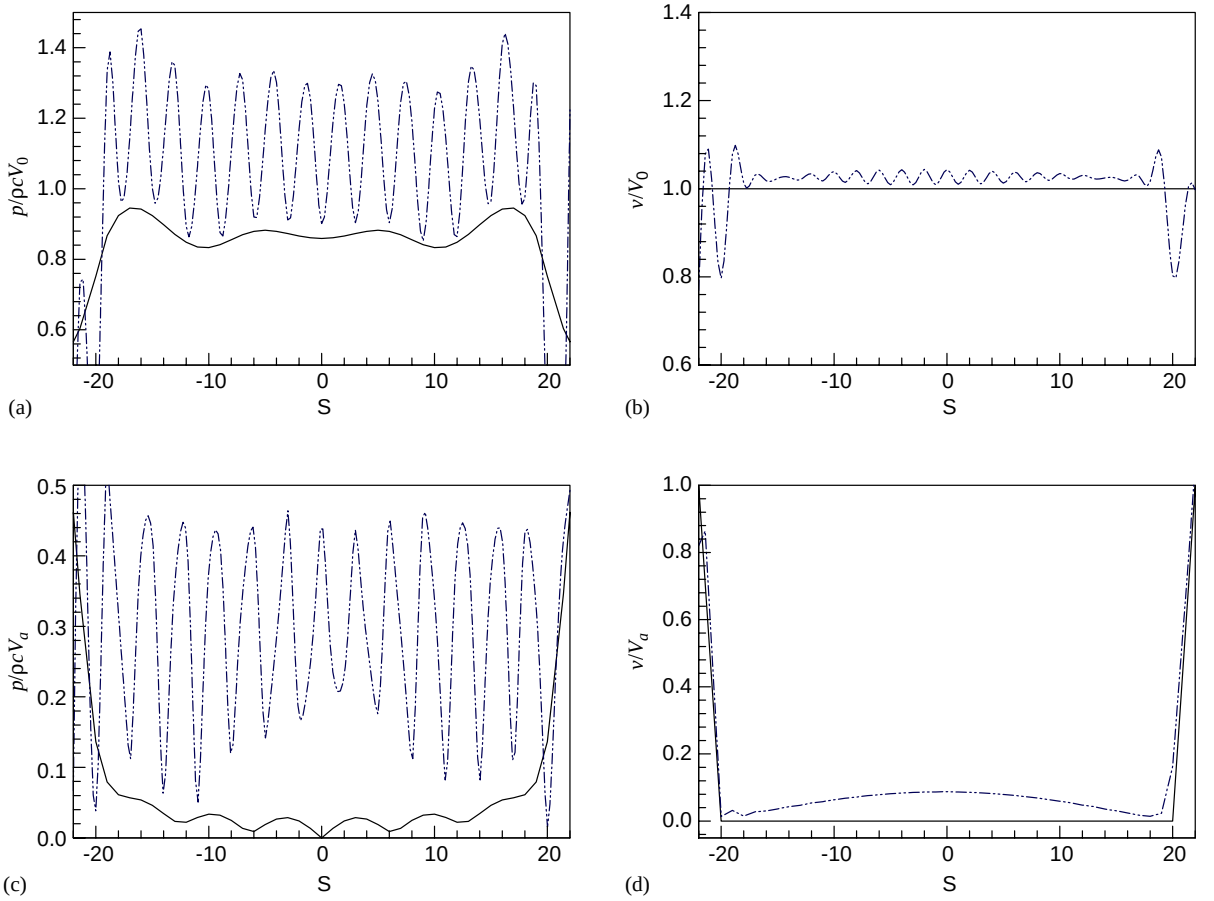

Fig. 9. Reconstructed dimensionless vibro-acoustic distributions on the surface of a dilating cylinder with two spherical endcaps and a large half-length to radius aspect ratio $b/a = 10$ at $ka = 1$ using IBEM alone with 506 discrete nodes and 253 measurements taken at a distance of 5 mm from the surface: — benchmark; – · · – IBEM. (a) Surface acoustic pressure for dilating case; (b) surface normal velocity for dilating case; (c) surface acoustic pressure for oscillating case; (d) surface normal velocity for oscillating case.

5. Conclusions

This study shows that hybrid NAH can be a very effective tool to diagnose the vibro-acoustic sources of a vibrating structure. It combines the advantages of both HELS and IBEM and allows for visualization of vibro-acoustic quantities on the surface of an arbitrarily shaped structure in a cost-effective manner. Since the majority of the input data are regenerated but not measured, the efficiency of reconstruction is enhanced. Meanwhile, the accuracy of reconstruction is guaranteed by the Helmholtz integral theory together with an optimal regularization and parameter choice methods. Hybrid NAH also enables one to identify the vibration modes that are responsible for acoustic radiation in the far field, which can provide great insight into vibro-acoustic diagnostics and noise suppression.

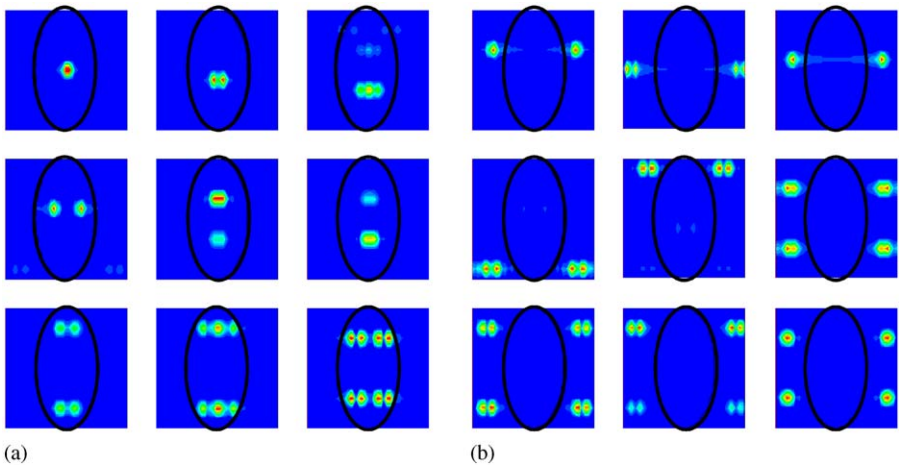

Fig. 10. Typical modes transformed into "k-space". The black circle represents the location of the radiation circle/ellipse (radius is the acoustic wave number $k = 10$). (a) Propagating modes; (b) evanescent modes.

Acknowledgements

This work was supported by an NSF Grant CMS-0245587.

References

[1] E.G. Williams, J.D. Maynard, Holographic imaging without the wavelength resolution limit, *Physical Review Letters* 45 (1980) 554–557.
[2] E.G. Williams, J.D. Maynard, E. Skudrzyk, Sound source reconstructions using a microphone array, *Journal of the Acoustical Society of America* 68 (1980) 340–344.
[3] E.G. Williams, H.D. Dardy, R.G. Fink, Near field acoustic holography using an underwater, automated scanner, *Journal of the Acoustical Society of America* 78 (1985) 789–798.
[4] E.G. Williams, The nearfield acoustic holography (NAH) experimental method applied to vibration and radiation in light and heavy fluids, *Computers and Structures* 65 (1997) 323–335.
[5] E.G. Williams, *Fourier Acoustics: Sound Radiation and Nearfield Acoustical Holography*, Academic Press, San Diego, 1999.
[6] W.A. Veronesi, J.D. Maynard, Digital holographic reconstruction of sources with arbitrarily shaped surfaces, *Journal of the Acoustical Society of America* 85 (1989) 588–598.
[7] G.V. Borgiotti, A. Sarkissian, E.G. Williams, L. Schuetz, Conformal generalized near-field acoustic holography for axisymmetric geometries, *Journal of the Acoustical Society of America* 88 (1990) 199–209.
[8] G.T. Kim, B.H. Lee, 3-D sound source reconstruction and field reprediction using the Helmholtz integral equation, *Journal of Sound and Vibration* 136 (1990) 245–261.
[9] M.R. Bai, Application of BEM (boundary element method)-based acoustic holography to radiation analysis of sound sources with arbitrarily shaped geometries, *Journal of the Acoustical Society of America* 92 (1992) 533–549.
[10] B.K. Kim, J.G. Ih, On the reconstruction of the vibro-acoustic field over the surface enclosing an interior space using the boundary element method, *Journal of the Acoustical Society of America* 100 (1996) 3003–3016.

[11] Z. Zhang, N. Vlahopoulos, S.T. Raveendra, T. Allen, K.Y. Zhang, A computational acoustic field reconstruction process based on an indirect boundary element formulation, *Journal of the Acoustical Society of America* 108 (2000) 2167–2178.
[12] H.A. Schenck, Improved integral formulation for acoustic radiation problems, *Journal of the Acoustical Society of America* 44 (1968) 41–58.
[13] S.C. Kang, J.G. Ih, Use of nonsingular boundary integral formulation for reducing errors due to near-field measurements in the boundary element method based near-field acoustic holography, *Journal of the Acoustical Society of America* 109 (2001) 1320–1328.
[14] Z. Wang, S.F. Wu, Helmholtz equation-least-squares method for reconstructing the acoustic pressure field, *Journal of the Acoustical Society of America* 102 (1997) 2020–2032.
[15] S.F. Wu, On reconstruction of acoustic pressure fields using the Helmholtz equation least squares method, *Journal of the Acoustical Society of America* 107 (2000) 2511–2522.
[16] N.E. Rayess, S.F. Wu, Experimental validations of the HELS method for reconstructing acoustic radiation from a complex vibrating structure, *Journal of the Acoustical Society of America* 107 (2000) 2955–2964.
[17] S.F. Wu, N. Rayess, X. Zhao, Visualization of acoustic radiation from a vibrating bowling ball, *Journal of the Acoustical Society of America* 109 (2001) 2771–2779.
[18] S.F. Wu, J. Yu, Reconstructing interior acoustic pressure field via Helmholtz equation least-squares method, *Journal of the Acoustical Society of America* 104 (1998) 2054–2060.
[19] M. Moondra, S.F. Wu, Visualization of vehicle interior noise using HELS based NAH, in: *Proceedings of the Inter-Noise 2002*, August 2002.
[20] N.E. Rayess, Development of Acoustic Holography using the Helmholtz Equation-least Squares (HELS) Method, Ph.D. Dissertation, Wayne State University, 2001.
[21] S.F. Wu, Hybrid nearfield acoustical holography, *Journal of the Acoustical Society of America* 115 (2004) 207–217.
[22] S.F. Wu, X. Zhao, Combined Helmholtz equation-least squares method for reconstructing acoustic radiation from arbitrarily shaped objects, *Journal of the Acoustical Society of America* 112 (2002) 179–188.
[23] I.N. Vekua, On completeness of a system of metaharmonic functions, *Doklady Akademii Nauk SSSR* 90 (5) (1953) 715–718 (in Russian).
[24] V. Isokov, S.F. Wu, On theory and application of the Helmholtz equation least squares method in inverse acoustics, *Inverse Problems* 18 (2002) 1147–1159.
[25] A.N. Tikhonov, On stability of inverse problems, *Doklady Akademii Nauk SSSR* 39 (1943) 176–179.
[26] N. Tikhonov, V.Y. Arsenin, *Solutions of Ill-posed Problems*, Wiley, New York, 1977, pp. 71–73 (Chapter 2).
[27] S. Twomey, On the numerical solution of Fredholm integral equations of the first kind by the inversion of the linear system produced by quadrature, *Journal of Association of Computing Machinery* 10 (1962) 97–101.
[28] P.C. Hansen, *Rank-Deficient and Discrete Ill-posed Problems*, SIAM, Philadelphia, PA, 1998.
[29] G.H. Golub, M. Heath, G. Wahba, Generalized cross-validation as a method for choosing a good ridge parameter, *Technometrics* 21 (1979) 215–223.
[30] E.G. Williams, Regularization methods for near-field acoustical holography, *Journal of the Acoustical Society of America* 110 (2001) 1976–1988.
[31] L. Landweber, An iteration formula for Fredholm integral equations of the first kind, *American Journal of Mathematics* 73 (1951) 615–624.
[32] V.A. Morozov, The error principle in the solution of operational equations by the regularization method, *USSR Computational Mathematics and Mathematical Physics* 8 (1968) 63–87.
[33] T. Semenova, On the Behavior of HELS Solutions for Acoustic Radiation and Reconstruction, Ph.D. dissertation, Department of Mechanical Engineering, Wayne State University, May 2004.